PAPER

Check for updates

Monolithic 3D micromixer with an impeller for glass microfluidic systems†

Sungil Kim, ‡[ab] Jeongtae Kim,‡[b] Yeun-Ho Joung,[b] Sanghoon Ahn,[a] Changkyoo Park,[a] Jiyeon Choi *[a] and Chiwan Koo *[b]

The performance of micromixers, namely their mixing efficiency and throughput, is a critical component in increasing the overall efficiency of microfluidic systems (*e.g.*, lab-on-a-chip and μ-TAS). Most previously reported high-performance micromixers use active elements with some external power to induce turbulence, or contain long and complex fluidic channels with obstacles to increase diffusion. In this paper, we introduce a new type of 3D impeller micromixer built within a single fused silica substrate. The proposed device is composed of microchannels with three inlets and a tank, with a mixing impeller passively rotated by axial flow. The passive micromixer is directly fabricated inside a glass plate using a selective laser-induced etching technique. The mixing tank, with its rotating shaft and 3D pitched blade impeller, exists within a micro-cavity with a volume of only 0.28 mm³. A mixing efficiency of 99% is achieved in mixing experiments involving three dye colours over flow rates ranging from 1.5–30 mL min⁻¹, with the same flow rates also applied to a sodium hydroxide-based bromothymol blue indicator and a hydrochloric acid chemical solution. To verify the reliable performance of the proposed device, we compare the mixing index with a general self-circulation-type chamber mixer to demonstrate the improved mixing efficiency achieved by rotating the impeller. No cracking or breakage of the device is observed under high inner pressures or when the maximum flow rate is applied to the mixer. The proposed microfluidic system based on a compact built-in 3D micromixer with an impeller opens the door to robust, highly efficient, and high-throughput glass-based platforms for micro-centrifuges, cell sorters, micro-turbines, and micro-pumps.

Introduction

Microfluidic devices (*e.g.*, lab-on-a-chip and μ-TAS) are attractive solutions when rapid 'point-of-care' (POC) testing with minimal consumption of the sample is required, such as in biological and chemical applications, medical diagnostics, food safety management, environmental monitoring, epidemics, and viral infections.[1–7] Therefore, to expedite the use of microfluidic devices, it is important to enable faster and more precise analysis and simple high-throughput systems by developing various fluid-control microfluidic platforms for sample weighing, reagent separation, mixing, reactions, and so on.[8] In particular, mixing elements such as micromixers are key aspects of microfluidic devices that are

used in pre-treatment steps in biochemical analysis, drug delivery, sequencing, and synthesis.[9,10] Mixing efficiency is the primary factor in determining the accuracy of detection and biochemical synthesis reactions. However, in the case of microfluidic devices, full mixing is difficult to achieve owing to a low Reynolds number.[11,12] Therefore, numerous studies have attempted to enhance the mixing efficiency by fabricating short mixing channels for compact integration and simple, automated fluid manipulation.[12–14]

Mixing channel platforms can be classified as passive mixers or active mixers depending on whether they require external power. Passive micromixers are composed of static components with no moving parts or power sources. Therefore, the system configuration is simple and the manipulation of fluid is easy. In general, reduction of the mixing volume or elongation of the microchannels for diffusion increases the mixing efficiency.[15–18] However, the reduced cross-section of microchannels with small mixing volumes is not suited to use in high-throughput devices, and elongation of the microchannel length is limited by standardized chip sizes. In addition, elongated microchannels in microfluidic devices normally increased

a Department of Laser and Electron Beam Technologies, Korea Institute of Machinery and Materials, Daejeon 34103, Republic of Korea.
E-mail: jchoi@kimm.re.kr
b Department of Electronics and Control Engineering, Hanbat National University, Daejeon 34158, Republic of Korea. E-mail: cwankoo@hanbat.ac.kr
† Electronic supplementary information (ESI) available. See DOI: 10.1039/d0lc00823k
‡ These authors contributed equally to this work.

hydraulic resistance; thus, their integration with other platforms is not straightforward, and high injection pressures may be required to ensure fluid flow in the microchannel. Therefore, a 3D flow channel structure has been proposed to enhance mixing efficiency.[17,18] The first demonstration of 3D flow using a serpentine structure was introduced by Liu *et al.* in 2000.[18] Following 3D flow demonstrations using zig-zag channels, obstacle structures and helical channels have been realized. The key idea of these devices is to maximize turbulence; however, they require complex channel design and complicated microelectromechanical systems (MEMS) fabrication techniques, including extended fabrication steps such as alignment and bonding.

Active mixers achieve high mixing efficiency by using external energy sources such as electro-kinetic flow, electrical fields, pressure, magnetic fields, and sound fields. In particular, active mixers using a rotating structure such as an impeller effectively eliminate laminar flow, enabling them to stir larger volumes through a short mixing channel.[16,19–26] Since the first demonstration of an impeller mixer using a micro-stirrer composed of a ferromagnetic material (Permalloy) by Lu *et al.* in 2001,[24] numerous studies have examined various impeller types without wire leads.[24–26] However, most of these impellers were metallic, and thus had poor chemical resistance in the cavity. Moreover, to embed an impeller inside the channel, the moving parts must be assembled separately.[20–26]

In this paper, we introduce a novel passive 3D impeller (3DI) micromixer that is more easily fabricated than conventional mixers and improves on their limited performance. The proposed device has three advantages. First, the impeller embedded in the micromixer can be driven by the injected flow from an external syringe pump. Thus, it does not require external power owing to its miniaturized and lightweight nature. This is a compact system with the potential for use in POC devices. Furthermore, the proposed impeller is a pitch blade type, which is more suitable for use in high-throughput processes than planar type impellers owing to its high mixing efficiency at fast flow rates. Second, all elements within the device, including the impeller, rotation shaft, and microchannels, are monolithically fabricated in a fused silica plate using a simple laser direct writing technique followed by chemical etching. Thus, complicated assembly processes are eliminated and the pressure resistance is improved. Third, the proposed micromixer is able to blend various chemical solutions because it is made of glass. Glass microfluidic devices exhibit high mechanical strength and chemical stability. Furthermore, in terms of reusability, glass devices are superior to organic polymers such as polydimethylsiloxane (PDMS) and polylactic acid, which are popular materials for microfluidic devices.[27–32]

The key technology used for the monolithic fabrication of the proposed device is selective laser-induced etching (SLE) (*i.e.*, femtosecond laser-assisted chemical etching and laser-assisted selective etching) based on ultrafast lasers. SLE is a mask-less two-step fabrication process comprising ultrafast laser direct writing and chemical wet etching.[33] It is one of the most flexible and reliable micro-structuring technologies for developing 'in-volume' 3D freeform structures inside transparent materials such as glass or sapphire.[34–37] SLE is superior to 3D printing based on organic polymers, as the latter is not suitable for manufacturing hollow structures such as microfluidic channels. For this reason, SLE technology is mainly used in the manufacture of dynamic fluid components such as 3D microfluidics and complex opto-fluidics.[28,32,38–40] Thus, it is clear that SLE is a powerful and unique fabrication method for 3D monolithic glass microfluidic devices.

Several passive micromixers with helical 3D microfluidic channels have been produced using SLE.[41–44] However, none of them has achieved both high mixing efficiency and high throughput. This is a technical drawback of SLE, because the wet etchant does not penetrate deeply into long microchannels. Thus, the length of microchannels fabricated by SLE is limited to a few millimetres. For complex microfluidic channels such as long helical channels, extra structures (*e.g.*, etchant access ports) may be required to improve the uniformity of diameters and pitches.[42–44]

In this work, we describe a novel 3DI micromixer that is monolithically fabricated by the SLE technique, and demonstrate its mixing efficiency using three different dyes. We also investigate the maximum mixing efficiency with high throughput using high-flow-rate acid and base solutions, and compare the performance of the device with that of conventional glass micromixer devices.

Experimental

Design and monolithic fabrication of 3DI mixer

The proposed micromixer includes a three-blade pitched impeller in a mixing zone (tank), three inlet channels separated by three layers, and an outlet channel. The detailed structure of the micromixer is shown in Fig. 1(A). As the impeller in the micromixer is operated passively by the flow of the injected fluid, the most important aspect of the design is to maximize the bulk motion effect. The 45° pitched blade impeller maximizes turbulence in the vortex structure; thus, it is advantageous to minimize the mixing time and isolated areas due to the effective elimination of a laminar flow.[45–48] Previous studies have shown that the shortest mixing time is achieved when the impeller and microchannels are of similar size.[26]

Furthermore, experimental offsets must be considered to achieve fabrication accuracy. For instance, the resolution scale of SLE, which is defined by the focus size of the laser beam, was taken into account in designing the 3D pitched blade impeller. Owing to the refractive index n of fused silica, the dimension of the mixer along the propagation direction of the writing beam had to be rescaled by $1/n$. In addition, material parameters such as the etching rate of the unmodified region and the optical absorption of the medium
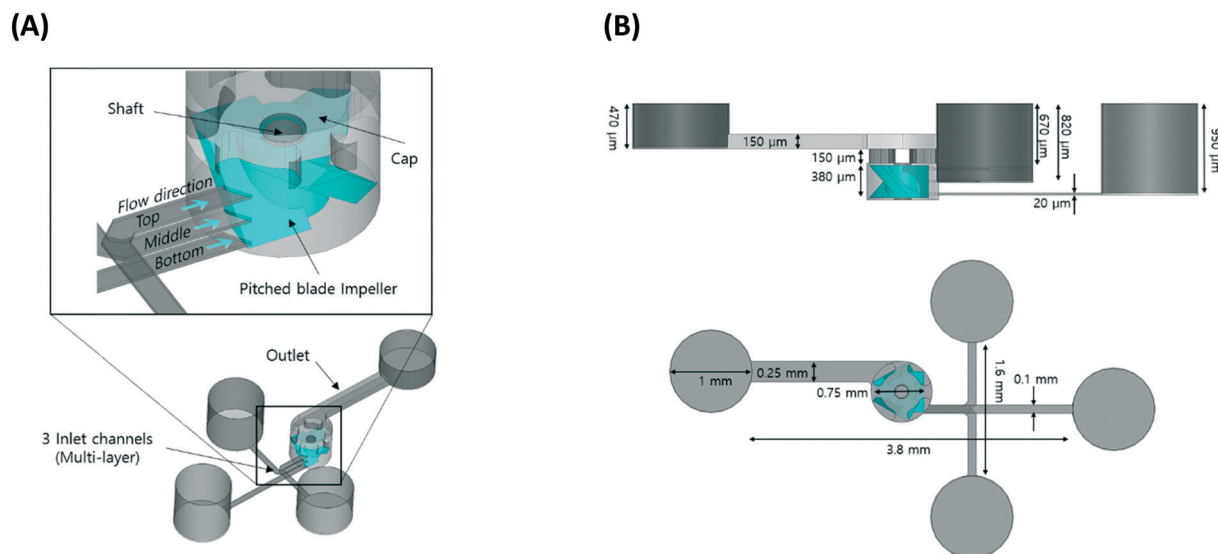
(A)

(B)

Fig. 1 (A) Schematic of the 3DI micromixer. (B) Side view and top view of the 3DI micromixer.

needed to be considered in the design. The aforementioned design rule for fused silica was empirically confirmed in our prior work on the fabrication of 3D multi-layer microfluidic channels.[49]

Therefore, the blade was designed with a width of 750 μm and a height of 380 μm so as to have a clearance of 15 μm from the walls and bottom of the mixing tank (width: 780 μm, height: 410 μm), thus minimizing the effects of wear and friction during rotation. A cross-shaped cap was added to prevent the impeller from moving from its original position.

The three independent inlet channels (20 μm depth, 100 μm width) were connected to the mixing tank at heights of 50, 190, and 330 μm from the bottom, respectively. The outlet channel was located at the top of the mixing tank, where the mixed flow leaves the device. The outlet channel width and depth were designed to be 250 μm and 150 μm, respectively, and the length of the channel was 3.8 mm. Details of the remaining channel dimensions are shown in Fig. 1(B).

The main procedure of device fabrication *via* SLE consists of two steps, as shown in Fig. 2. First, a focused laser beam

with a pulse width of approximately 1 ps is exposed within a glass plate. During this process, owing to nonlinear absorption, the material only absorbs photon energy in the vicinity of the focal point, causing the material to be locally modified.[39] Second, the modified part is selectively removed by chemical etching. The etching rate of the laser-modified area is much higher than that of the unexposed area, enabling us to obtain sufficient etching selectivity beyond 300 : 1.[49]

An ultrafast laser-based (Satsuma HP2, Amplitude laser) 3D laser structuring system was used to directly write microchannels inside a glass substrate (fused silica, JMC glass), with dimensions of 10 mm × 10 mm × 2 mm. The laser beam, deflected using a two-axis (*XY*) Galvano scanner (DynAXIS, SCANLAB GmbH), was finally focused through an objective lens (NA 0.42, Mitutoyo M plan Apo 50×). The glass substrate was mounted on a three-axis air-bearing motion stage operated by a controller (A3200, AEROTECH) and 3D fabrication software (3Dpoli, Femtika). The laser modification parameters (wavelength: 1030 nm,
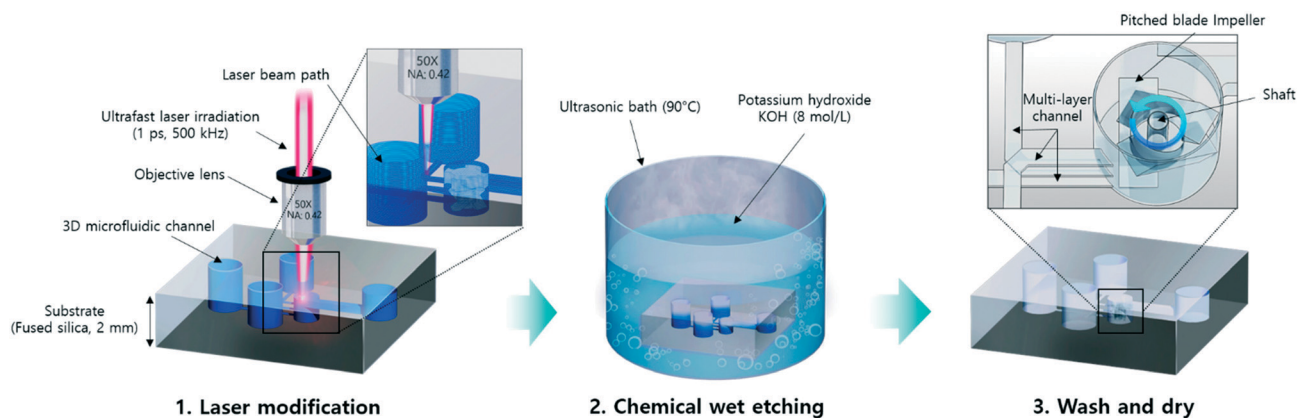

Fig. 2 Fabrication steps for the 3DI micromixer using selective laser-induced etching.

repetition rate: 500 kHz, pulse energy: 400 nJ, scan rate: 200 mm s^{-1}, slicing and hatching size: 10 μm and 15 μm, respectively) were optimized as described in our previous research.[49] The modified substrate was immersed in an ultrasonic bath of potassium hydroxide (8 mol L^{-1}) at 90 °C, and finally cleaned with isopropyl alcohol, deionized (DI) water, and nitrogen gas.

Conditions for rotation of the 3D impeller

As the 3DI micromixer is a passive device, the 3D impeller is rotated by the force that results from the flow of solutions injected into the microchannels. Thus, the 3DI micromixer requires a minimum flow rate to overcome the friction between the impeller and the rotation axis and initiate rotation of the impeller. As shown in Fig. 3 (experiment 1), DI water was injected into the 3DI micromixer to determine the minimum flow rate. Three 10 mL syringes were filled with DI water and connected to the inlets of the 3DI micromixer with Tygon tubing. The outlet of the 3DI micromixer was connected to a waste bottle. After tubing, the 3DI micromixer was placed on the stage of an optical microscope, and water was infused into it using a syringe pump (Fusion 100, Chemyx) over a range of flow rates. To obtain the minimum flow rate for revolving the impeller, the flow rate of the syringe pump was steadily increased from 0.1 to 1.0 mL min^{-1} in 0.1 mL min^{-1} steps, and the rotation of the micro impeller was recorded using a video camera (DS-Ri2, Nikon) integrated with the microscope. The total flow rate of mixing solutions running through the mixing tank was three times the flow rate setting on the pump, because solutions from three syringes on the pump were injected into the three inlets of the 3DI micromixer. The total flow rate was used to describe the injection speed of the solutions to be mixed.
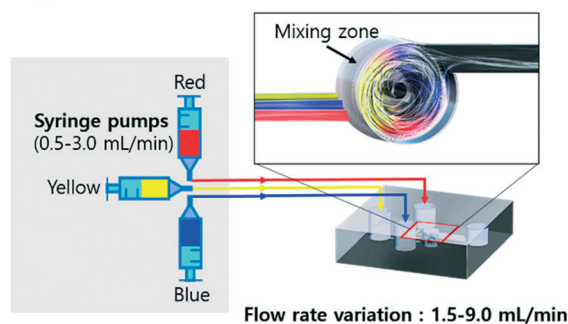
Mixing efficiency

Three dyes were injected into the inlets and the mixing efficiency in the microfluidic channel after the tank was observed; the results are shown in Fig. 3 (experiment 2). Three syringes loaded on a syringe pump and containing red, yellow, and blue dyes, respectively, were connected to the 3DI micromixer device through Tygon tubing. To observe the dependence of the mixing efficiency of the 3DI micromixer on the flow rate of the inserted fluid, the flow rates of the dyes were increased from 1.5 to 9.0 mL min^{-1} in 1.5 mL min^{-1} steps.

The mixing of the dyes was monitored and captured by a microscope camera connected to a computer. To analyse the mixing performance quantitatively, red, green, and blue intensity information for each pixel was extracted from the microscopy images over a range of 0–400 μm from the mixing chamber. Approximately 200 data points per distance were sampled. The intensity of each pixel was used to determine the average of the three colour intensities.[50] The intensity data were converted to mixing index (MI) values using eqn
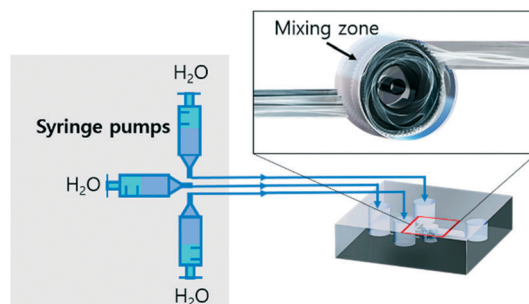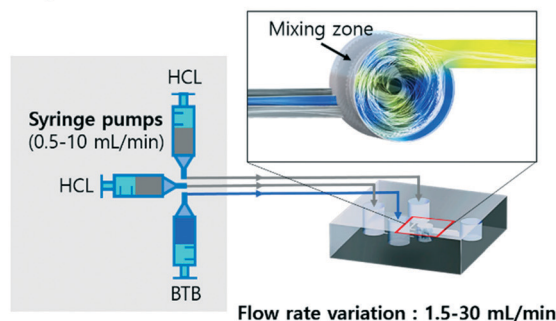

Fig. 3 Schematic of three-step validation of the performance of the 3DI micromixer. Experiment 1: flow rate measurements for the rotation of the micro impeller, experiment 2: mixing efficiency at total flow rates ranging from 1.5–9.0 mL min^{-1}, experiment 3: performance test of the mixing throughput of chemical fluids at total flow rates ranging from 1.5–30 mL min^{-1}.

(1), where I_k is the intensity of the kth pixel, $\bar{I}_o$ is the mean intensity, and N is the total number of pixels. MI is the ratio of the standard deviation to the mean of the intensity.[51]

$$\mathrm{MI} = 1 - \frac{\sqrt{\frac{1}{N}\sum_{k=1}^{k=N}(I_k - \bar{I}_0)^2}}{\bar{I}_0} \qquad (1)$$

MI can never be zero because the intensity in the unmixed condition is not zero. However, there will be some minimum value. Similarly, MI cannot be one in the fully mixed condition because of the backlight. Thus, to show the mixing efficiency clearly, the calculated MIs were analysed in relative terms using the minimum and maximum MI values. The calculated MI was renormalized according to the minimum and maximum MI values using eqn (2), where MI_n is the normalized MI, MI_k is the calculated MI, MI_{max} is the maximum MI, and MI_{min} is the minimum MI. For the normalized MI, 0 indicates unmixed and 1 indicates fully mixed.

$$MI_n = \frac{MI_k - MI_{min}}{MI_{max} - MI_{min}} \tag{2}$$

Chemical mixing and throughput performance

Our 3DI micromixer was able to mix a variety of chemical solutions because it was fabricated on a glass substrate. Glass has very high chemical resistance compared with PDMS, which is widely used for the fabrication of microfluidic devices. To verify the stable chemical mixing performance of the 3DI micromixer, basic and acidic solutions were selected for subsequent experiments.

Fig. 3 (experiment 3) shows the setup for chemical mixing. In the experiment, hydrochloric acid (HCl) and sodium hydroxide (NaOH) were used. To verify how well the acid and basic solutions were blended, bromothymol blue (BTB) pH indicator was selected; this substance is often used in applications to measure the pH of a solution in the range 6–7.6. As an acidic solution is blended with BTB, the colour of the mixture gradually changes from blue to greenish-blue and finally to yellow. A 0.1% (g/v) BTB solution in NaOH was prepared by mixing 1 g of BTB powder (DSP-1019, DUKSAN) in 70% (v/v) ethanol and 2.5 mL of a 0.1 M NaOH solution. When using 0.01 M HCl, the colour of a 1 : 1 mixture of the HCl solution and the BTB solution changed to yellow. As shown in step 3 in Fig. 3, the 3DI micromixer had three inlets; the 0.005 M HCl solution was injected through two channels, and the BTB solution through the other. The colour of the mixture was observed using the camera while the solutions were injected with the syringe pump. Flow rates from 1.5–9 mL min^{-1} in steps of 0.5 mL min^{-1} were tested. In addition, high flow rates of 15 and 30 mL min^{-1} were tested for high-throughput performance evaluation. The maximum flow was limited to 30 mL min^{-1} by the injection force of the syringe pump and the bonding force between the connection tubing and the micromixer.

Results and discussion

Component of 3DI micromixer

Using SLE, all the device elements were monolithically prototyped in a glass chip without further assembly. Fig. 4(A)
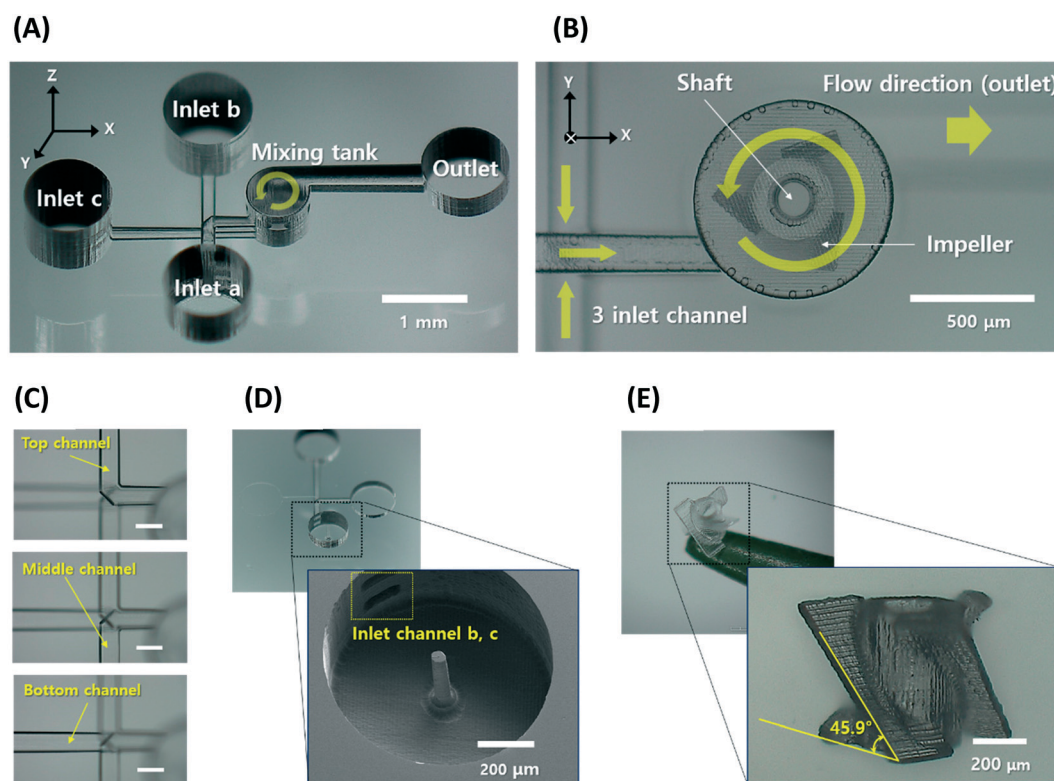
Fig. 4 Fabricated 3DI micromixer using selective laser-induced etching. (A) 3D optical microscopy image of three-port multi-layered inlet channels, a single mixing tank, and a single outlet. (B) Bottom view of the mixing tank. (C) Top view of the multi-layered inlet channels (scale bar is 150 μm). (D) Scanning electron microscopy image of the mixing tank (micro impeller has been removed). (E) 3D optical microscopy image of the pitched blade impeller.

shows 3D digital microscopy images (KH-8700, Hirox) of an isometric view of the 3DI micromixer. The micromixer measures 6 mm (length) × 1.04 mm (height), and possesses a mixing tank, three inlets, and one outlet. As shown in the bottom view of the mixing tank (Fig. 4(B)), the impeller in the mixing tank has three pitched blades, with a gap of 30 μm between the end of the blade and the inner wall of the mixing tank. This clearance is required to prevent blade breakage during rotation and to maximize the bulk motion effect on the liquids to be mixed. Fig. 4(C) shows top views of the three multi-layered inlet channels, which are separated by ~170 μm without any through holes or connections. Each inlet channel has dimensions of 130 μm (width) × 60 μm (height), and the outlet channel itself measures 300 μm (width) × 250 μm (height). Fig. 4(D) shows an optical microscopy image of the 3DI micromixer after removing the top cover of the mixing tank. The enlarged image is a scanning electron micrograph (SEM) of the mixing tank with the shaft that serves as a rotation axis for the impeller. The shaft, which stands on the tank bottom like the other elements, was monolithically fabricated by SLE without any additional bonding process. Thus, SLE was expected to confer mechanical strength on the 3DI micromixer parts, ensuring the durability of the device even under high-pressure conditions such as the injection of tens of millilitres (macro-scale) of fluid. Fig. 4(D) also shows that the inner surface of the mixing tank has been formed smoothly, without any defects or bumps. Fig. 4(E) shows a micro pitched impeller taken off the shaft. The impeller measures 720 μm (width) × 550 μm (height). The pitched blade is very thin and small, but there are no microcracks or defects on the surface. The blades have an angle of 45.9°, almost the same as that specified in the design, because of the high accuracy of SLE when producing complicated 3D structures. The total process time was 25.5 h, including 1.5 h for laser writing to draw the 3D shapes and 24 h for full chemical wet etching of the laser-modified inner structures. The average wet etching rate of the laser modified area was estimated to be 130 μm h^{-1}.

The average roughness of three points (in a region of 50 μm × 50 μm) on the wall surface of the outlet channel was determined to be about 200 nm by atomic force microscopy (XE7, Park Systems) measurements. This indicates sufficient surface quality to generate a laminar flow in the microchannel.[52,53]

Minimum operating flow rate and colour mixing efficiency

The total flow rate inside the 3DI micromixer was initially set to 0.3 mL min^{-1} and gradually increased by 0.3 mL min^{-1} until the impeller started rotating. Below 1.5 mL min^{-1}, the impeller did not rotate, and the water passed by the mixing tank and flowed through the outlet channel (Fig. 5(A)). At 1.5 mL min^{-1}, the impeller began to rotate (Fig. 5(B)). At flow rates above 1.5 mL min^{-1}, the impeller rotated faster. The
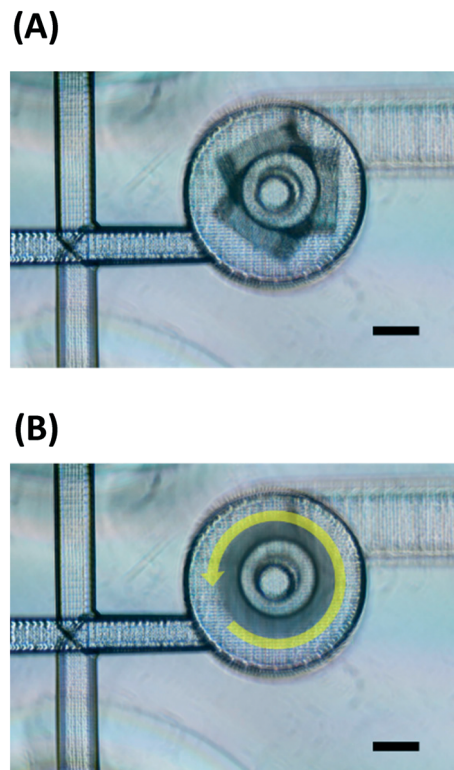

(A)

(B)

Fig. 5 Microscopy image of the impeller inside the mixing tank. (A) Stopped impeller. (B) Rotating impeller. Yellow arrow shows the direction of fluidic flow (scale bar is 200 μm).

rotation speed of the impeller was not analysed in this work because the microscope camera could only capture 12 frames per second.

The mixing performance at various flow rates was analysed using red, yellow, and blue dyes. At low flow rates, such as 1.5, 3, or 4.5 mL min^{-1}, the dyes were not fully mixed, and red and green colours were observed in the outlet channel region (Fig. 6(A–C)). As shown in Fig. 6(A), at 1.5 mL min^{-1}, a green colour resulting from the mixture of yellow and blue dyes was observed along the wall of the channel, and a red stream flowed along the other wall. At the boundary between the green and red streams, a dark (almost black) colour was observed due to mixing based on diffusion. The area of the dark colour increased as the dyes flowed away from the mixing tank. At 3 and 4.5 mL min^{-1}, the green and red colours decreased and appeared almost fully mixed (Fig. 6(B) and (C)). At flow rates above 6 mL min^{-1}, the dyes were fully mixed, as shown in Fig. 6(D–F).

To quantitatively evaluate the mixing efficiency of the 3DI micromixer, the MI was calculated using the average intensities of red, green, and blue extracted from the captured microscopy images. The intensity information of the pixels was extracted through the vertical lines on the outlet channel of the 3DI micromixer, which were placed at 100 μm intervals up to 400 μm from the out-port of the mixing tank, as shown in Fig. 6(A). After acquiring intensity information for all three colours, the values were averaged to give the final intensity data, with MI calculated using eqn (1)
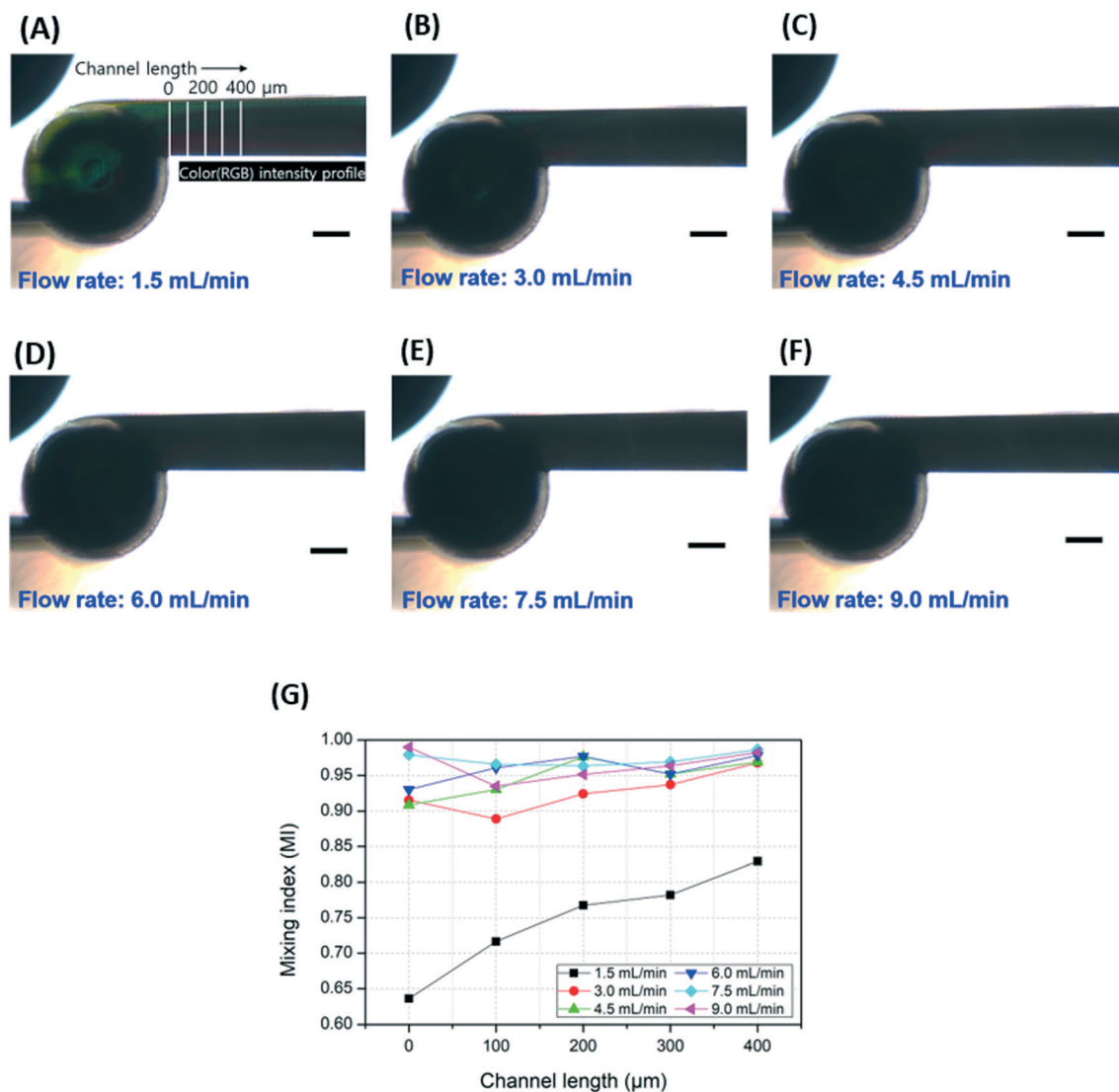
Fig. 6 (A–F) Microscopy images of injection of red, yellow, and blue dyes at flow rates of 1.5, 3.0, 4.5, 6.0, 7.5, and 9.0 mL min^{-1} (scale bar is 200 μm). (G) Graph of mixing index *versus* channel length for the flow rates shown in parts A–F. vertical yellow lines in A are the data extraction lines. Pixel data were extracted at 100 μm intervals up to 400 μm.

and normalized using eqn (2). A graph of MI *versus* distance from the mixing chamber (channel length) is shown in Fig. 6(G). At 1.5 mL min^{-1}, the MI value increased from 0.64 to 0.83 as the distance from the mixing tank increased from 0 to 400 μm. When using flow rates equal to or greater than 3 mL min^{-1}, the MI value (excluding that observed 100 μm away from the mixing tank at 3 mL min^{-1}) was greater than 0.9. In addition, the MI value tended to increase as the channel length increased. It was difficult to find a linear equation to fit the relationship between the flow rate and the MI, but there was a trend of increasing MI at higher flow rates.

Although our 3DI micromixer achieved good mixing performance in the three-dye mixing test, the microscopy images do not display significant differences. As mentioned above, there is some absorption of backlight. Thus, the brightness and contrast of the microscopy images were adjusted to ensure significant differences before the red,

green, and blue intensity information was extracted. Fig. 6(A–F) are adjusted images, but the differences cannot be clearly distinguished by the naked eye. In addition, the inlets of our micromixer were completely separated, so that the dyes could not mix in the area of the inlet channels. However, as shown in Fig. 7, the area where the inlet channels overlap appears black. Thus, if vertical laminar flow remains even after passing through the mixing tank, the outlet channel will appear black. As a result, it is thought that the mixing results may be inaccurate when using image analysis to evaluate the mixing of three colour dyes.

Chemical mixing efficiency and high-throughput performance

In previous studies, the mixing performance of a micromixer has been evaluated using the colour reaction of an indicator
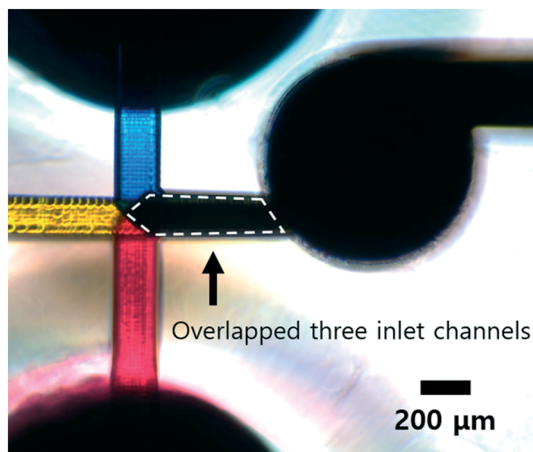
Fig. 7 Microscopy image of the inlet area in front of the mixing chamber. White dashed line shows the overlapped area of the three inlet channels. Although the channels were physically separated, the overlapped area appears black as the three dyes become mixed.

such as phenolphthalein to an acid base.[42–44] However, in the case of phenolphthalein, both acidic and neutral

reactions are colourless, so there is a limit to confirming the exact mixing process and performance. Therefore, we conducted accurate colour analysis with a chemical mixing test using a BTB indicator that reacts to both acidic, neutral, and alkaline. As shown in Fig. 8(A), the BTB solution was injected through the middle-layer channel, and HCl solution was injected through the top- and bottom-layer channels. The BTB streamline (blue colour) appeared on the upper side of the outlet channel, and the remaining area had a greenish colour. This indicates that the BTB solution was at least 50% blended with the HCl solution. Up to 3 mL min^{-1}, the width of the BTB solution streamline decreased and the area of the greenish colour was diminished, as shown in Fig. 8(B–D). As the flow rate increased, the blue streamline almost disappeared, and the mixture became dark yellow in all areas of the outlet channel, as shown in Fig. 8(E and F). At 9.0 mL min^{-1}, the blue stream faded away and the mixture became bright yellow, as shown in Fig. 8(G). Under high flow rate conditions such as 15 or 30 mL min^{-1}, there was no damage or leak in the micromixer device, and the solutions were blended well (Fig. 8(H and I)). Thus, this micromixer is a candidate for efficient high-throughput mixing.
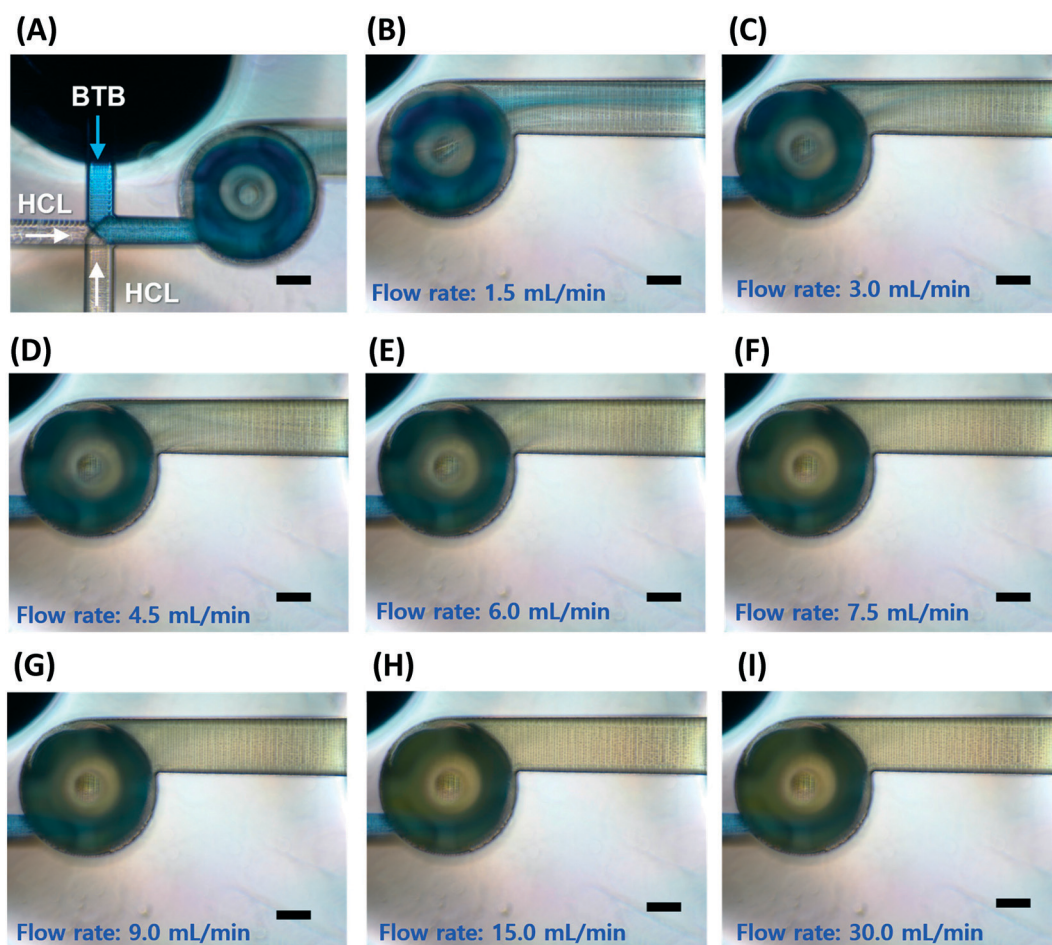
Fig. 8 Microscopy images of mixing with the BTB pH indicator in NaOH solution and HCl solution. (A) Inlets of the 3DI micromixer. The BTB solution was injected through one inlet channel and the HCl solution was injected through the other two. (B–I) Mixing results for flow rates of 1.5, 3.0, 4.5, 6.0, 7.5, 9.0, 15.0, and 30.0 mL min^{-1} (scale bar is 200 μm).

(A)

(B)

(C)
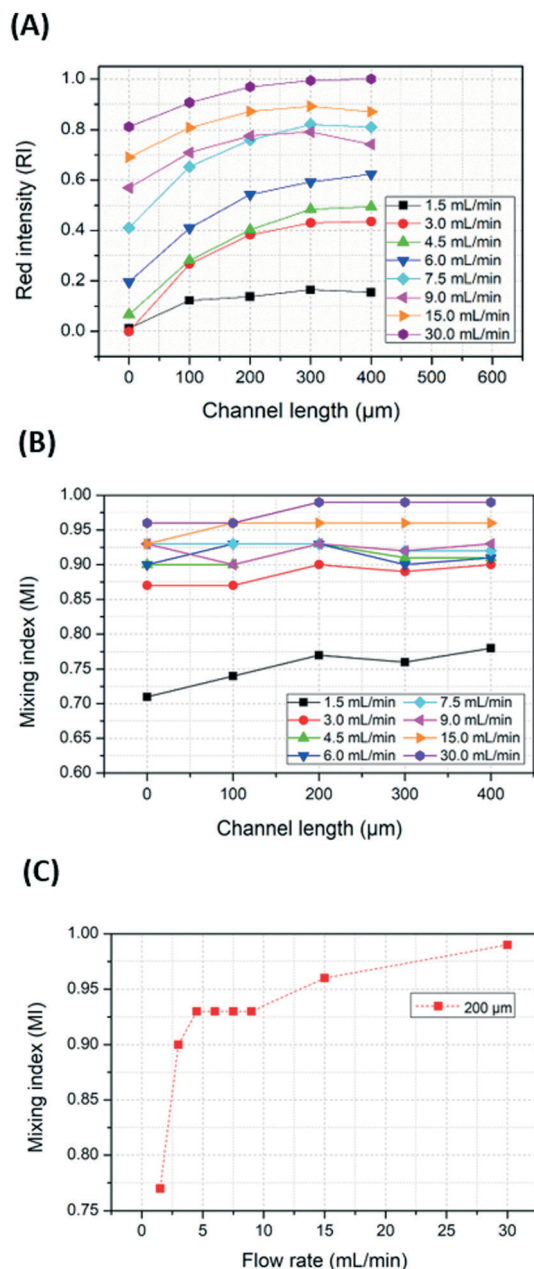
Fig. 9 (A) Graph of normalized red intensity (RI) according to flow rate and distance from the mixing tank. As RGB intensity for yellow could not be extracted, the mixing performance was analysed using the RI of the yellow component. (B) Graph of mixing index values from the greyscale images. (C) Mixing efficiency at 200 μm away from the mixing tank for each flow rate.

As described in the Experimental section, owing to the change of the BTB solution colour from blue to yellow as the HCl solution was mixed, the red intensity (RI) of the images gradually increased, because yellow has red and green colour components, whereas blue does not. Fig. 9(A) shows the normalized RI with respect to flow rate and distance from the mixing tank. As the flow rate increased, the mixing performance improved owing to the high rotation speed of the impeller, resulting in an increased RI. In particular, RI

increased rapidly at distances above 200 μm and flow rates greater than 3 mL min⁻¹. However, an increase in the distance at a flow rate of 9 ml min⁻¹ or higher did not significantly change the RI. It was difficult to find a linear equation to fit the relationship between the flow rate and the RI, similar to the mixing efficiency trend observed in the previous three-dyes test.

To quantitatively evaluate the mixing performance of the micromixer for the BTB and HCl solutions, the MI was calculated from the recorded images. The microscopy images were changed to greyscale images to better distinguish yellow from blue, as these two colours are similar in RGB intensity, making it hard to calculate the MIs for the change in the BTB solution from yellow from blue. Fig. 9(B) shows the MI graph for the chemical mixing test. At 1.5 mL min⁻¹, the MI was about 0.7 and tended to increase with distance from the mixing tank (channel length). When the flow rate increased from 1.5 to 3 mL min⁻¹, the MI jumped from 0.7 to about 0.85, an increase of 0.15. As the flow rate increased to more than 3 mL min⁻¹, the MI gradually increased. At flow rates greater than 3 mL min⁻¹, the MIs were at least 0.9. These results are similar to those obtained in the three-dye mixing test. As mentioned above, at flow rates greater than 3 mL min⁻¹, the BTB and the HCl solution were fully mixed, and the BTB solution became bright yellow. In addition, most of the calculated MI values were greater than 0.95, verifying the high mixing performance at 15 mL min⁻¹ and 30 mL min⁻¹. At 30 mL min⁻¹, the mixing efficiency increased to 99% at 200 μm from the mixing tank. Therefore, our 3DI micromixer exhibits strong repeatability, regardless of the type of solution.

As shown in Fig. 9(C), however, the MI over a specific channel section of 200 μm was maintained at flow rates of 4.5–9.0 mL min⁻¹, but exhibited an overall linear increasing trend, different from the colour dye mixing results. This is because the full mixing colour was yellow, which is observable without image correction. As a result, the mixing experiments using BTB indicators were not affected by backlight absorption, thus improving the inaccurate results of the colour dye experiments and enabling accurate analysis of the mixing efficiency.

Rapid mixing with high mixing efficiency is required for a high-throughput mixer.[54] Although a typical passive micromixer has limited high-throughput ability, our 3DI micromixer provides rapid mixing performance and high mixing efficiency.

To closely analyse the impact of the impeller on mixing performance, an additional 3DI micromixer without an impeller was fabricated for comparison. Fig. 10 shows the results for the 3DI micromixers with and without impellers. The 3DI micromixer without an impeller is similar to a mixer with only a circular mixing tank. Previous studies have demonstrated effective mixing by Dean-vortices in circular mixing tanks using self-circulation.[55] However, to improve its efficiency, the device must be configured with multiple mixing tanks, and so it needs to be longer or bigger. As
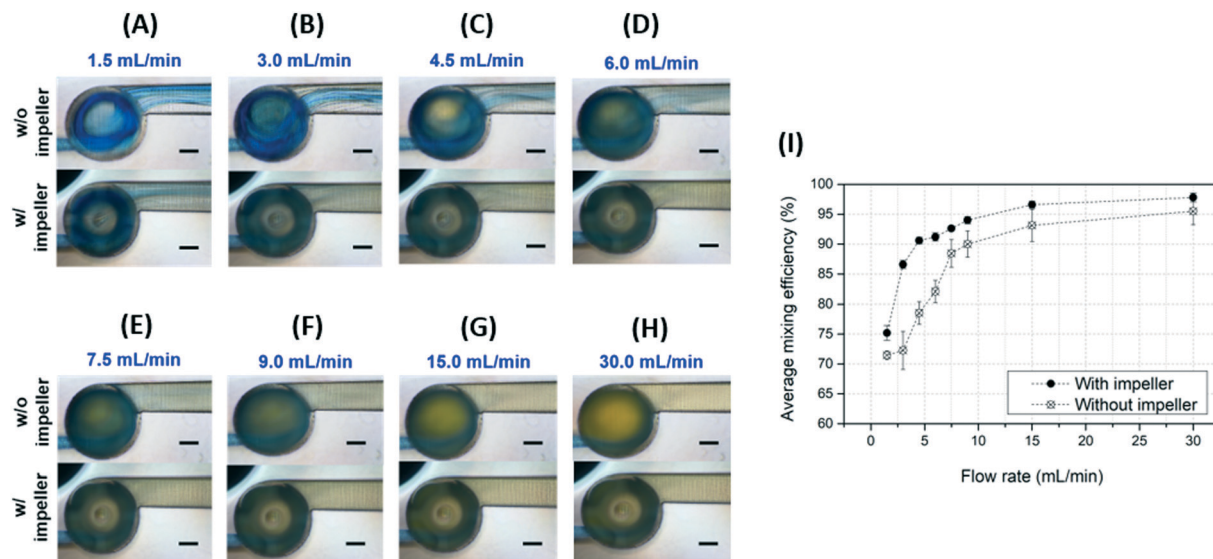
Fig. 10 (A–H) Microscopy images of the mixing comparison of the 3D micromixer with the impeller and the one without an impeller at flow rates of 1.5, 3.0, 4.5, 6.0, 7.5, 9.0, 15.0, and 30.0 mL min^{-1}, respectively (scale bar: 200 μm). (I) Graph of the average mixing efficiency for each flow rate.

shown in Fig. 10(A) and (B), the blue streamline after the 3DI micromixer with the impeller was narrower than that formed without an impeller at flow rates of 1.5 and 3.0 mL min^{-1}. With flow rates of 4.5, 6.0, 7.5, and 9.0 mL min^{-1}, the streamlines after the 3DI micromixer with the impeller were almost yellowish, while the mixer without an impeller still produced a blue streamline (Fig. 10(C–F)). Better mixing performance was achieved by the impeller rotation of the 3DI micromixer. However, at flow rates of 15 and 30 ml min^{-1}, the streamlines after the mixer without an impeller also became yellowish, as shown in Fig. 10(G and H). However, there was some difference in brightness between the mixers with and without an impeller. For further investigation mixing performance, the average mixing efficiency over a distance of 0–400 μm was calculated using MI from the captured images and plotted with respect to flow rate, as shown in Fig. 10(I). At all tested flow rates (from 1.5–30.0 mL min^{-1}), the average mixing efficiency in the 3DI micromixer with the impeller was greater than in the mixer without an impeller. Thus, the impeller in the micromixer affects the mixing performance positively. Note, however, that the average mixing efficiency difference at the highest flow rate of 30.0 mL min^{-1} was relatively small, and the effect of the impeller was relatively weak while the effect of turbulence became stronger. Thus, these results confirm that the 3DI

micromixer with an impeller offers better mixing performance than without, except for the flow rate of 30 ml min^{-1}, and that a longer channel is not required.

A comparison of the different 3DI micromixers reported over the past three years is presented in Table 1. Our device had a mixing channel length that is 180 μm longer than the 3D helical mixer investigated using the same process, but did not require processing of extra parts and achieved a 4% increase in mixing efficiency.[44] In addition, the proposed fabrication method does not require a high-temperature bonding process,[56,57] and provides throughput performance five times higher than the maximum flow rate previously reported.[58]

Interestingly, the 3DI micromixer showed stable mixing as the impeller rotated faster at a high flow rate. Typical polymer devices using PDMS-to-PDMS bonding or PDMS-to-glass bonding have low pressure resistance. One limitation of mixing performance when using high flow rates is a high risk of breakage due to weak bonding strength. A microfluidic device using glass-to-glass bonding is better optimized for high-pressure experiments than a PDMS-based device, but glass-to-glass hermetic sealing is not straightforward.[59] Our device was 3D-fabricated in-volume glass without any bonding; thus, it has excellent pressure resistance and higher durability than devices fabricated from polymers such as

Table 1 Comparison of performance of glass-based passive micromixers studied over the past three years (2018–2020)

Channel length to reach maximum mixing efficiency (mm)	Maximum mixing efficiency (%)	Flow rate (μL min^{-1})	Process	Glass type
0.8 (ref. 44)	95	3.3	SLE (3D) with extra access ports	Fused silica
23.5 (ref. 56)	90	300	Wet etching + hot press bonding	Soda-lime
111 (ref. 57)	N/R	0.2	Moulding + thermal fusion bonding	Soda-lime
5.5 (ref. 58)	N/R	6000	SLE (2D) + catalysis bonding	Fused silica
0.98 (this work) mixing tank (0.78) + outlet channel (0.2)	**99**	**30 000**	**SLE (3D)**	**Fused silica**

PDMS, which is widely used for the fabrication of microfluidic devices. The proposed device is fully embedded in the glass substrate and does not require assembly. Although it was not possible to measure the maximum flow rate owing to the performance limitations of the syringe pump system and the internal pressure limit on the tubing, even when a maximum flow rate of 30 mL min^{-1} was injected, the 3DI micromixer was robust without leakage to the fluidic channel or the mixing tank.

Specifically, our device has been evaluated in terms of mixing performance under very harsh experimental conditions. First, dyes were injected at six flow rates of up to 9 mL min^{-1}, then BTB and chemical solutions were injected at various flow rates of up to 30 mL min^{-1}. During the experiments, rinsing was repeatedly performed at the maximum flow rate of 30 mL min^{-1} to ensure the inside of the fluidic channel and tank remained clean. Therefore, 30 or more fluid injections were required to evaluate device performance. Based on the flow rate and fluid channel volume information, it is possible to calculate the approximate revolutions per minute (RPM) of the impeller. Even after approximately 1 million revolutions of the impeller blades over 10 hours, no degradation of mixing performance or damage was observed. As a result, the durability of the built-in glass parts is an advantage only in monolithic fabrication using SLE.

Conclusions

This work, to the best of the authors' knowledge, demonstrates the first 3D micromixer with an impeller embedded in fused silica. It was fabricated using ultrafast laser-based SLE technology, *via* a simple and intuitive, yet powerful, fabrication method. First, three-dye mixing tests were carried out to observe the mixing efficiency of the 3DI micromixer. Images of the mixing of dyes were acquired by a microscope equipped with a digital camera. For quantitative analysis of the mixing efficiency, the MI was calculated using pixel data extracted from the microscopy images. The 3DI micromixer operates in a passive way, because the micro impeller rotates according to the flow of the injected fluids. In the mixing performance test, the MI values were greater than 0.9 (mixing efficiency 90%), except at the flow rate of 1.5 mL min^{-1}.

Owing to its high chemical resistance, the glass-based 3DI micromixer enables the use of a variety of chemical solutions that are not compatible with polymer materials such as PDMS. As a demonstration of a chemical mixing application, the NaOH-based BTB pH indicator and HCl solution were mixed successfully with high efficiency and high throughput. The native blue colour of the BTB indicator nearly disappeared at a distance of 200 μm from the mixing tank when using a flow rate of 3 mL min^{-1}. When using flow rates above 4.5 mL min^{-1}, the mixture turned yellow immediately after the mixing tank.

When we compared the 3DI micromixer with the impeller to one without an impeller, the effect of the impeller was observed to produce an improvement of 2–14% in average mixing efficiency over the chamber-type mixer. However, with the 30 mL min^{-1} flow rate, the effect of the impeller became diminished and the effect of turbulence became stronger. The mechanical properties of the base material of the impeller were not altered by SLE because the exterior of the structure was removed by laser modification followed by etching. Therefore, the device can endure high inner pressures due to high flow rates of up to 30 mL min^{-1}. To conclude, the demonstrated 3DI micromixer is a strong candidate for use in glass microfluidic platforms with free-standing rotatable structures generating a vortex stream, such as micro-centrifuges, cell sorters, micro-turbines, and micro-pumps.

Author contributions

Conceptualization: S. K., J. K. methodology: S. K., J. K. project administration: Y.-H. J. validation: S. A., C. P. investigation: S. A., C. P. formal analysis: S. K., J. K. visualization: S. K. data curation: J. K. writing original draft: S. K., J. K. writing review & editing: J. C., C. K. Supervision: J. C., C. K. funding acquisition: J. C., S. A., C. K.

Conflicts of interest

There are no conflicts to declare.

Acknowledgements

References

1 G. M. Whitesides, *Nature*, 2006, **442**, 368–373.
2 A. K. Yetisen, M. S. Akram and C. R. Lowe, *Lab Chip*, 2013, **13**, 2210–2251.
3 A. Trautmann, G. L. Roth, B. Nujiqi, T. Walther and R. Hellmann, *Microsyst. Nanoeng.*, 2019, **5**, 1–9.
4 L. Y. Hung, T. B. Huang, Y. C. Tsai, C. S. Yeh, H. Y. Lei and G. B. Lee, *Biomed. Microdevices*, 2013, **15**, 539–551.
5 J. Zhuang, J. Yin, S. Lv, B. Wang and Y. Mu, *Biosens. Bioelectron.*, 2020, **163**, 112291.
6 J. Zhang, B. Gharizadeh, D. Lu, J. Yue, M. Yu, Y. Liu and M. Zhou, *IEEE Rev. Biomed. Eng.*, 2020, DOI: 10.1109/RBME.2020.2991444.
7 A. D. Beaton, C. L. Cardwell, R. S. Thomas, V. J. Sieben, F. Legiret, E. M. Waugh, P. J. Statham, M. C. Mowlem and H. Morgan, *Environ. Sci. Technol.*, 2012, **46**, 9548–9556.
8 G. Cai, L. Xue, H. Zhang and J. Lin, *Micromachines*, 2017, **8**, 274.
9 C. D. Chin, T. Laksanasopin, Y. K. Cheung, D. Steinmiller, V. Linder, H. Parsa, J. Wang, H. Moore, R. Rouse, G. Umviligihozo, E. Karita, L. Mwambarangwe, S. L. Braunstein,

J. van de Wijgert, R. Sahabo, J. E. Justman, W. El-Sadr and S. K. Sia, *Nat. Med.*, 2011, **17**, 1015–1019.

10   A. J. DeMello, *Nature*, 2006, **442**, 394–402.

11   T. M. Squires and S. R. Quake, *Rev. Mod. Phys.*, 2005, **77**, 977.

12   A. J. Conde, I. Keraite, A. E. Ongaro and M. Kersaudy-Kerhoas, *Lab Chip*, 2020, **20**, 741–748.

13   M. Bayareh, M. N. Ashani and A. Usefian, *Chem. Eng. Process.*, 2020, **147**, 107771.

14   M. M. Aeinehvand, F. Ibrahim, S. W. Harun, I. Djordjevic, S. Hosseini, H. A. Rothan, R. Yusof and M. J. Madou, *Biosens. Bioelectron.*, 2015, **67**, 424–430.

15   A. Bertsch, S. Heimgartner, P. Cousseau and P. Renaud, *Lab Chip*, 2001, **1**, 56–60.

16   V. Hessel, H. Löwe and F. Schönfeld, *Chem. Eng. Sci.*, 2005, **60**, 2479–2501.

17   A. D. Stroock, S. K. Dertinger, A. Ajdari, I. Mezić, H. A. Stone and G. M. Whitesides, *Science*, 2002, **295**, 647–651.

18   R. H. Liu, M. A. Stremler, K. V. Sharp, M. G. Olsen, J. G. Santiago, R. J. Adrian, H. Aref and D. J. Beebe, *J. Microelectromech. Syst.*, 2000, **9**, 190–197.

19   G. S. Jeong, S. Chung, C. Kim and S. Lee, *Analyst*, 2010, **135**, 460–473.

20   S. Yu, T. Jeon and S. M. Kim, *Chem. Eng. J.*, 2012, **197**, 289–294.

21   M. R. Rasouli and M. Tabrizian, *Lab Chip*, 2019, **19**, 3316–3325.

22   N. Veldurthi, S. Chandel, T. Bhave and D. Bodas, *Sens. Actuators, B*, 2015, **212**, 419–424.

23   L. Yang, J. Cheng, P. Fan, C. Yang and Z. Mao, *Chem. Eng. Technol.*, 2013, **36**, 443–449.

24   L. Lu, K. S. Ryu and C. Liu, *Micro Total Analysis Systems*, 2001, pp. 28–30.

25   J. Atencia and D. J. Beebe, *Proceedings of the 7th international conference on micro total analysis systems*, 2003, pp. 5–9.

26   K. S. Ryu, K. Shaikh, E. Goluch, Z. Fan and C. Liu, *Lab Chip*, 2004, **4**, 608–613.

27   K. L. Wlodarczyk, D. P. Hand and M. M. Maroto-Valer, *Sci. Rep.*, 2019, **9**, 1–13.

28   K. Sugioka, J. Xu, D. Wu, Y. Hanada, Z. Wang, Y. Cheng and K. Midorikawa, *Lab Chip*, 2014, **14**, 3447–3458.

29   F. Sima, K. Sugioka, R. M. Vázquez, R. Osellame, L. Kelemen and P. Ormos, *Nanophotonics*, 2018, **7**, 613–634.

30   T. Su, K. Cheng and Y. Sun, *Microsyst. Technol.*, 2019, **25**, 4399–4403.

31   J. Choi and C. Schwarz, *Int. J. Appl. Glass Sci.*, 2020, **11**, 480–490.

32   R. Osellame, H. J. Hoekstra, G. Cerullo and M. Pollnau, *Laser Photonics Rev.*, 2011, **5**, 442–463.

33   A. Marcinkevičius, S. Juodkazis, M. Watanabe, M. Miwa, S. Matsuo, H. Misawa and J. Nishii, *Opt. Lett.*, 2001, **26**, 277–279.

34   K. Sugioka, Y. Hanada and K. Midorikawa, *Laser Photonics Rev.*, 2010, **4**, 386–400.

35   J. Gottmann, M. Hermans and J. Ortmann, *Phys. Procedia*, 2012, **39**, 534–541.

36   D. Wortmann, J. Gottmann, N. Brandt and H. Horn-Solle, *Opt. Express*, 2008, **16**, 1517–1522.

37   L. Capuano, R. Pohl, R. M. Tiggelaar, J. W. Berenschot, J. Gardeniers and G. Römer, *Opt. Express*, 2018, **26**, 29283–29295.

38   G. Meineke, M. Hermans, J. Klos, A. Lenenbach and R. Noll, *Lab Chip*, 2016, **16**, 820–828.

39   K. Sugioka and Y. Cheng, *Light: Sci. Appl.*, 2014, **3**, e149.

40   N. Burshtein, S. T. Chan, K. Toda-Peters, A. Q. Shen and S. J. Haward, *Curr. Opin. Colloid Interface Sci.*, 2019, **43**, 1–14.

41   Y. Liao, J. Song, E. Li, Y. Luo, Y. Shen, D. Chen, Y. Cheng, Z. Xu, K. Sugioka and K. Midorikawa, *Lab Chip*, 2012, **12**, 746–749.

42   S. He, F. Chen, K. Liu, Q. Yang, H. Liu, H. Bian, X. Meng, C. Shan, J. Si and Y. Zhao, *Opt. Lett.*, 2012, **37**, 3825–3827.

43   K. Liu, Q. Yang, S. He, F. Chen, Y. Zhao, X. Fan, L. Li, C. Shan and H. Bian, *Microsyst. Technol.*, 2013, **19**, 1033–1040.

44   C. Shan, F. Chen, Q. Yang, Z. Jiang and X. Hou, *Micromachines*, 2018, **9**, 29.

45   M. Schäfer, M. Yianneskis, P. Wächter and F. Durst, *AIChE J.*, 1998, **44**, 1233–1246.

46   M. F. Distelhoff, A. J. Marquis, J. M. Nouri and J. H. Whitelaw, *Can. J. Chem. Eng.*, 1997, **75**, 641–652.

47   F. Cabaret, L. Fradette and P. A. Tanguy, *Chem. Eng. Technol.*, 2008, **31**, 1806–1815.

48   I. Torotwa and C. Ji, *Designs*, 2018, **2**, 10.

49   S. Kim, J. Kim, Y. Joung, S. Ahn, J. Choi and C. Koo, *Micro and Nano Systems Letters*, 2019, **7**, 1–7.

50   H. Fu, X. Liu and S. Li, *RSC Adv.*, 2017, **7**, 10906–10914.

51   H. C. Tekin, V. Sivagnanam, A. T. Ciftlik, A. Sayah, C. Vandevyver and M. A. Gijs, *Microfluid. Nanofluid.*, 2011, **10**, 749–759.

52   J. Gottmann, M. Hermans, N. Repiev and J. Ortmann, *Micromachines*, 2017, **8**, 110.

53   S. Ameer-Beg, W. Perrie, S. Rathbone, J. Wright, W. Weaver and H. Champoux, *Appl. Surf. Sci.*, 1998, **127**, 875–880.

54   T. Luong, V. Phan and N. Nguyen, *Microfluid. Nanofluid.*, 2011, **10**, 619–625.

55   A. Alam and K. Kim, *Sens. Actuators, B*, 2013, **176**, 639–652.

56   H. Shi, K. Nie, B. Dong, L. Chao, F. Gao, M. Ma, M. Long and Z. Liu, *Chem. Eng. J.*, 2019, 123642.

57   M. R. Haq, Y. K. Kim, J. Kim, J. Ju and S. Kim, *J. Micromech. Microeng.*, 2019, **29**, 075010.

58   J. Qi, W. Li, W. Chu, J. Yu, M. Wu, Y. Liang, D. Yin, P. Wang, Z. Wang, M. Wang and Y. Cheng, *Micromachines*, 2020, **11**, 213.

59   S. Kim, J. Kim, Y. Joung, J. Choi and C. Koo, *Micromachines*, 2018, **9**, 639.